Herz, Andreas; Franz, Anna; Theska, Felix; Hentschel, Martin; Kups, Thomas; Wang, Dong; Schaaf, Peter:

Solid-state dewetting of single- and bilayer Au-W thin films: unraveling the role of individual layer thickness, stacking sequence and oxidation on morphology evolution

Original published in:

AIP Advances. - New York, NY : American Inst. of Physics. - 6 (2016), 3, art. 035109, 10 p.

ISSN: 2158-3226

DOI: 10.1063/1.4944348

URL: http://dx.doi.org/10.1063/1.4944348

[Visited: 2016-06-14]

Solid-state dewetting of single- and bilayer Au-W thin films: Unraveling the role of individual layer thickness, stacking sequence and oxidation on morphology evolution

A. Herz, A. Franz, F. Theska, M. Hentschel, Th. Kups, D. Wang, and P. Schaaf

Citation: AIP Advances **6**, 035109 (2016); doi: 10.1063/1.4944348
View online: http://dx.doi.org/10.1063/1.4944348
View Table of Contents: http://scitation.aip.org/content/aip/journal/adva/6/3?ver=pdfcov
Published by the AIP Publishing

Solid-state dewetting of single- and bilayer Au-W thin films: Unraveling the role of individual layer thickness, stacking sequence and oxidation on morphology evolution

A. Herz,[a] A. Franz, F. Theska, M. Hentschel, Th. Kups, D. Wang,[a] and P. Schaaf

Department of Materials for Electronics and Electrical Engineering, Institute of Materials Science and Engineering and Institute of Micro- and Nanotechnologies MacroNano®, TU Ilmenau, D-98693 Ilmenau, Germany

(Received 12 January 2016; accepted 2 March 2016; published online 11 March 2016)

Self-assembly of ultrathin Au, W, and Au-W bilayer thin films is investigated using a rapid thermal annealing technique in an inert ambient. The solid-state dewetting of Au films is briefly revisited in order to emphasize the role of initial film thickness. W films deposited onto SiO_2 evolve into needle-like nanocrystals rather than forming particle-like agglomerates upon annealing at elevated temperatures. Transmission electron microscopy reveals that such nanocrystals actually consist of *tungsten (VI) oxide* (WO_3) which is related to an *anisotropic oxide crystal growth* out of the thin film. The evolution of W films is highly sensitive to the presence of any residual oxygen. Combination of both the dewetting of Au and the oxide crystal growth of WO_3 is realized by using various bilayer film configurations of the immiscible Au and W. At low temperature, Au dewetting is initiated while oxide crystal growth is still suppressed. Depending on the stacking sequence of the Au-W bilayer thin film, W acts either as a substrate or as a passivation layer for the dewetting of Au. Being the ground layer, W changes the wettability of Au which clearly modifies its initial state for the dewetting. Being the top layer, W prevents Au from dewetting regardless of Au film thickness. Moreover, regular pattern formation of Au-WO_3 nanoparticles is observed at high temperature demonstrating how bilayer thin film dewetting can create unique nanostructure arrangements. [http://dx.doi.org/10.1063/1.4944348]

I. INTRODUCTION

Solid-state dewetting (SSD) of metallic thin films is well known as a simple and effective way to obtain tailored micro- and nanostructures for potential applications in catalysis, ecology, information technology, or plasmonics.[1–5]

SSD of Au thin films has been investigated in a number of studies.[6–10] A comprehensive view on the microstructural evolution of *continuous films* is provided by Müller and Spolenak.[11] Upon annealing, it is found that void as well as grain growth in the film correlate with (111) intensities of X-ray diffraction. This change in intensity can be used to trace the dewetting. Depending on Au film thickness (and the type of the substrate), morphology evolution and final particle size distribution will be different:[12] An increasing layer thickness gives rise to continuous films after deposition and, upon annealing, bigger particles are formed which are less dense-packed on the substrate.[13] In the present work, a brief review on the influence of Au film thickness on morphology evolution will be given.

[a]Authors to whom correspondence should be addressed. Electronic mail: andreas.herz@tu-ilmenau.de, dong.wang@tu-ilmenau.de

W films are barely investigated with respect to SSD. To the best of our knowledge, the only report on W dewetting or self-assembly available in literature was found in Liu *et al.*[14] Here it is stated that needle-like W nanocrystals form at temperatures below 1000 °C upon annealing for 2 min in an inert ambient out of ultrathin W films deposited on SiO_2. At higher temperatures, this anisotropic effect, *i.e.*, different growth rates along different crystal orientations vanishes due to an increased mobility of surface mobile atoms. However, any systematic study on this effect and the combination with the dewetting of another metal is missing.

Recently, SSD of multi-component thin films comprising Au alloys have been studied, revealing individual features with respect to the alloying element: Anisotropic hole growth is found to occur in quasi-single crystalline Au/Fe bilayers accompanied by a considerably high thermal stability compared to its polycrystalline Au counterpart.[15] Au-Pt films also show a delay in thermal agglomeration upon alloying small amounts of Pt to the Au film.[7] In case of Au/Ni bilayers, phase separation and void evolution is found to be crucial during SSD.[16] Another study uses a sacrificial antimony layer.[17] In a comprehensive case study, the effect of individual layer thickness and stacking sequence on the SSD of Au-Co bilayer thin films has been shown.[18] All these findings may be understood as an approach to modify the dewetting nature of Au.

An additional case is presented in this work. Au and W single- and bilayer thin films provide an interesting situation: The melting point of W (3422 °C) is considerably higher than that of Au (1064 °C) and different cubic crystal systems are present for W (body-centered cubic, bcc) and Au (face-centered cubic, fcc). Consequently, from thermodynamics, this binary system is *completely immiscible* in solid state. Individual layers as well as bilayers are studied and compared within the scope of this work. For the bilayer configurations considered, the role of stacking sequence at low temperature will be highlighted. For W being the ground layer, the substrate effect which depends on initial Au film thickness is shown. W being on top is shown to hinder the dewetting of Au due to passivation. Influencing parameters associated with SSD, such as activation energies for void initiation/void growth, diffusion paths being active, or ambient conditions are discussed with respect to changes in film morphology. Furthermore, it is demonstrated that the combination of Au and W thin film evolution can be used to make regular arrays of nanoparticles (NPs).

II. MATERIALS AND METHODS

A. Film deposition

Au and W single- and bilayer thin films were deposited onto a p-type silicon substrate (6–10 Ω cm), which was (100) oriented. Prior to deposition, a 90 nm thick oxide barrier layer was thermally grown onto the Si in order to avoid any interaction between substrate and layer material. For optical measurements, fused silica was used as the substrate for film deposition. Electron beam evaporation at a base pressure of 2×10^{-7} mbar was used for deposition of Au and W. Deposition accuracy was determined to be approximately 5% of film thickness. Au films had a variable thickness of 1, 2.5, 3, 5, and 10 nm. The layer thickness of W was fixed at 3 nm. Corresponding Au/W bilayer systems were 3/3 and 10/3 (in nm) with Au as the top layer. The same was done in reversed order (with W being the top layer).

B. Thermal treatment

Rapid thermal annealing (RTA, *Jipelec Jetstar 100*) was carried out at different temperatures (180, 320, 520, 550, 700, 750, 900, and 950 °C). Before annealing, the RTA chamber was pumped and purged with N_2 several times in order to ensure adequate purity. Forming gas flow at ambient pressure (Ar-3.3% H_2, 6N purity) was further applied to prevent samples from contamination during thermal treatment. After annealing, samples were cooled to room temperature in the furnace.

C. Characterization

The morphology of the as-deposited and as-annealed samples was investigated by high-resolution scanning electron microscopy (SEM, *Hitachi S-4800*). Low (2 kV) acceleration voltage was applied in order to minimize charging. Secondary (SE) as well as backscattered electron (BSE) imaging were used to reveal sample features. Feature sizes were calculated using the tool *analyze particles* of the free software *ImageJ*.[19] For this purpose, SEM micrographs were converted into binary images by setting a threshold. X-ray diffraction (XRD, *Siemens D-5000*) was carried out in Bragg-Brentano (BB) geometry using Cu Kα irradiation at 40 kV in a parallel beam optic. Nanomanipulation was performed using *Kleindiek*® MM3A-EM micromanipulators being mounted in the focused ion beam device (FIB, *Zeiss Auriga 60 crossbeam*) to cleanly transfer nanostructures onto a TEM grid. For adequate observation, these objects were put on a 300 mesh Cu grid with a two-layer graphene film on a lacey carbon film, provided by Plano GmbH, Wetzlar, Germany. Transmission electron microscopy (TEM, *FEI Tecnai 20 S-Twin*) was used in combination with energy-dispersive X-ray spectroscopy (STEM-EDS). Optical measurements were performed using a UV-Vis spectrometer in transmission mode (Agilent Cary 5000 UV-Vis-NIR).

III. RESULTS AND DISCUSSION

A. Formation of Au NPs through dewetting revisited

Figure 1 illustrates that, depending on Au film thickness, the as-deposited state significantly affects mean size, areal density and morphology of the Au NPs formed. For 3 nm Au, a discontinuous film of *isolated* Au islands is grown; lateral grain growth or -evolution in such multi-grained island structures is limited. This implicates that initial steps for the dewetting in solid state (*i.e.*, void formation and -evolution) are skipped when transforming the polycrystalline islands into single- or bi-crystal particles. This is of course quite contrary to *continuous films* where film voids and grain boundaries are found to interact.[11,20] Consequently, uniform spherical Au NPs are formed rather fast via surface (and/or interface) diffusion upon annealing at elevated temperature. Surface melting

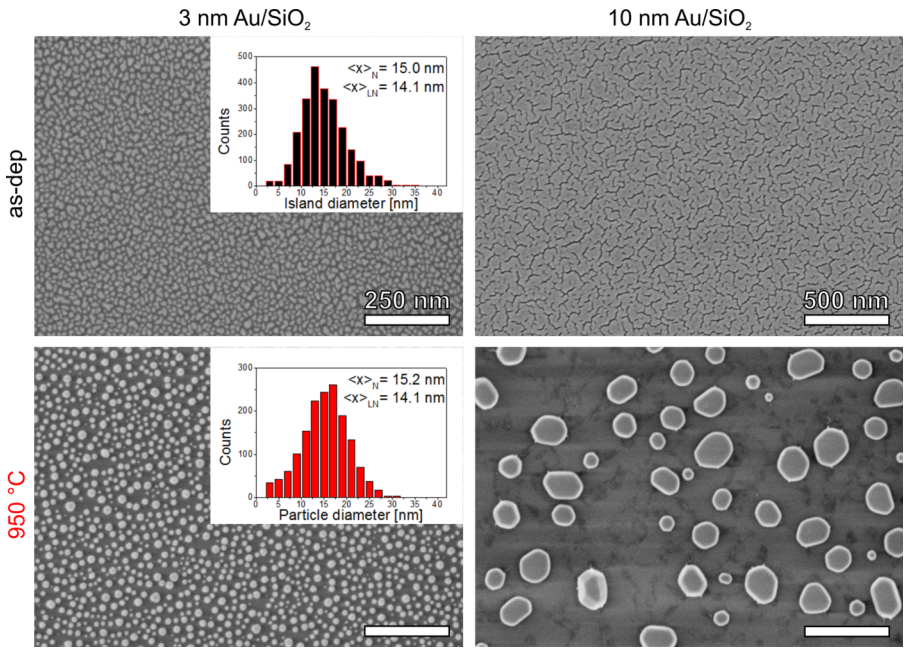

FIG. 1. NP formation via SSD of Au thin films deposited on SiO_2. Both samples were annealed for 1 min at 950 °C. Statistical analyses on mean feature size using normal ($<x>_N$) or lognormal ($<x>_{LN}$) PDF are shown for 3 nm Au for the purpose of comparison. It is seen that NP characteristics are determined by the as-deposited state ("as-dep"). Scale bars are valid down the column.

may also contribute here due to reduced scale. Particle mean diameter coincides with the one of the former Au islands, indicating that common void evolution and associated reallocation of film material did not occur. However, long-term annealing may cause the mean particle size to increase due to ripening of densely populated particles. Such a phenomenon is indeed reported for ultrathin Au films annealed at 900 °C for 60 min.[8]

For 10 nm Au, the as-deposited state is a continuous layer with *grooves* running through it (Figure 1). These grooves are probably caused by some residual stresses inside the film after deposition. Anyway, this morphology causes the dewetting to turn into a different mode. The majority of the particles formed by dewetting are rather flat showing faceted edges. This metastable shape even holds for long-term annealing (in case of not containing grain boundaries).[21] Moreover, the (lateral) particle size is considerably higher than in case of the 3 nm Au film. A clear view of particle size evolution as a function of Au film thickness during SSD on SiO_2 is given elsewhere.[13] The main message here is the fact that Au film evolution (and final particle formation) is predefined by its initial state after deposition, especially for ultrathin Au films with a layer thickness well below 10 nm. An immediate consequence is observed for the plasmonic nature of the Au nanostructures considered. Figure 2 exemplarily shows UV-Vis spectra of ultrathin Au films: A clear blue-shift of the localized surface plasmon resonance peak is observed for temperatures above 320 °C which occurs due to the dewetting of isolated islands into spherical NPs already at low temperatures. This shape effect becomes more evident at increasing initial film thickness. Here, the aspect ratio of the island network also increases until structures interconnect. This trend becomes visible in Figure 2. The transformation of high-aspect ratio nano-islands into nano-spheres then results in a larger peak shift. A more rigorous examination can be found elsewhere.[22]

B. Morphology evolution of W thin films

A completely different behavior is found for W thin films (Figure 3(a)). The agglomeration starts from a *continuous and closed* W layer. Here, a grainy surface is visible from image contrast in the SEM micrograph. Even small seed-like structures can be identified, possibly acting as starting points for the self-assembly: Generally speaking, dewetting means that film material agglomerates in such a way that the film gradually exposes the underlying substrate via evolution of crystal voids. However, upon annealing, ultrathin W films show a kind of nanocrystal growth instead. At 550 °C, small nanorods (NRs) start growing from the top of the film without building voids. Their spatial arrangement seems to be random. At increasing temperature, some remaining film material is also transformed into NPs and the aspect ratio of the ultrafine needles becomes extensively higher, indicating anisotropic crystal growth along a preferred crystal axis.

In order to clarify this assumption, high-resolution TEM investigations were performed. Figure 3(b) exemplarily shows the transport of an individual NR from the original SiO_2 substrate onto a TEM grid. It can be confirmed that such a single crystalline NR reveals a preferred growth direction which is shown in Figure 3(c). However, lattice spacing does not match any crystallographic plane of the bcc W. It rather coincides with the spacing of $(0\ 2\ 0)_m$ of the monoclinic *tungsten (VI) oxide* (WO_3),[23] which is a low-symmetry system. Reduced crystal symmetry of WO_3 may facilitate spontaneous, anisotropic growth: In the monoclinic system, one of the axes is superior in such a way that it is perpendicular to the other two axes, allowing crystal growth along a preferential direction. Oxide formation is also evident from STEM-EDS where a considerable amount of oxygen was detected (compared to the signal coming from W). This agglomeration mechanism is contrary to the assumption to be a dewetting mode. In fact, thinking of the considerably high melting point of W, it can be related to an anisotropic oxide crystal growth from small seeds out of the W film in the presence of any residual oxygen. Oxidation may result from impurities during deposition and/or annealing and, moreover, from pre-existing adsorbate states of the pure W surface as samples were exposed to air between both processes.[24]

C. Morphology evolution of Au-W bilayer thin films

Four different scenarios are considered when putting the evolution of Au and W thin films together: The stacking sequence as well as individual Au film thickness are combined to investigate

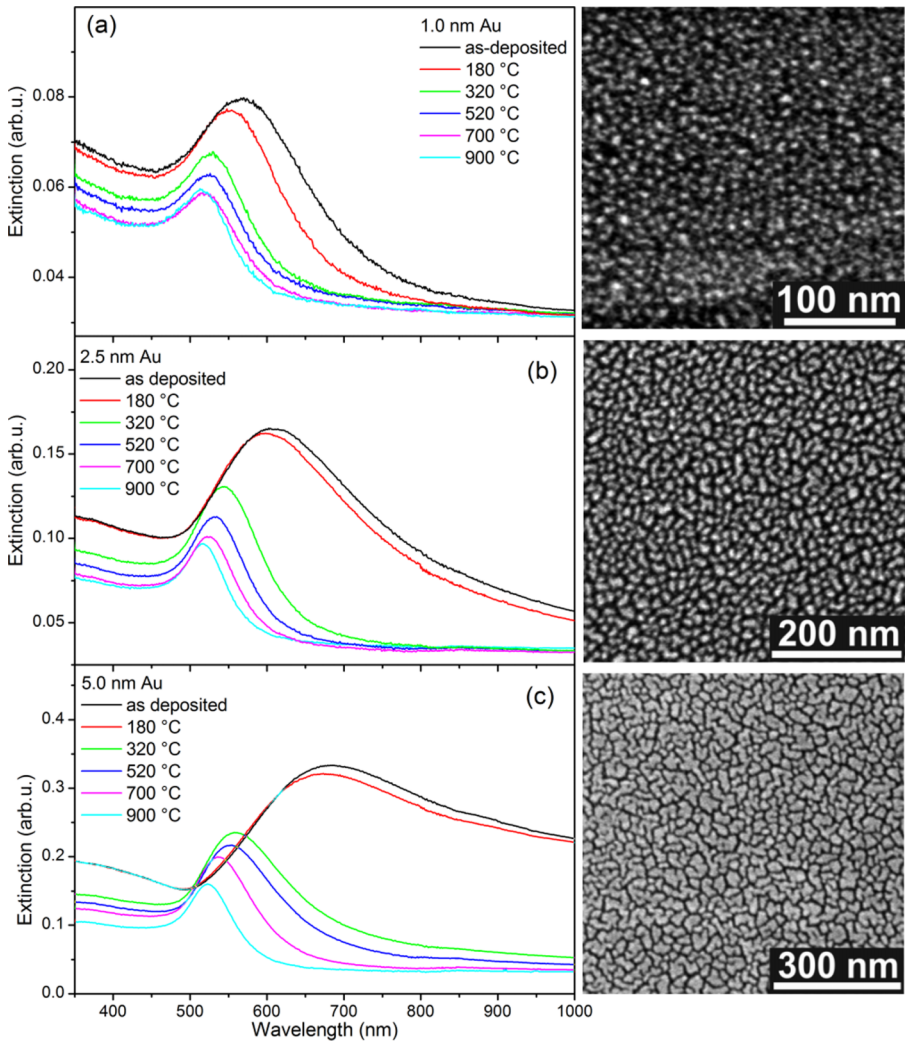

FIG. 2. Extinction spectra of ultrathin Au films deposited on fused silica as a function of film thickness. Temperature dependence of the localized surface plasmon resonance peak can be related to the transformation of isolated Au islands in the as-deposited state into spherical NPs upon dewetting. This wavelength shift increases with increasing initial film thickness. Short-term annealing (30 sec) was conducted for all thermal treatments (a – c). Additionally, SEM micrographs of corresponding as-deposited states are also provided to the right of each spectrum.

the SSD of the immiscible Au-W binary system at low temperature. Furthermore, morphology evolution at high temperature will be observed to possibly reveal a certain interaction between the NP formation of Au as well as the oxide nanocrystal growth of W thin films.

1. Low temperature annealing – Au dewetting modified

In Figure 4, all Au as well as Au-W thin film arrangements are illustrated. For a 3 nm Au thin film deposited on SiO_2 it is seen that particle characteristics are already established upon low temperature annealing: Spherical NPs which are similar in size and shape like the ones formed at 950 °C are found (Figure 1). However, Au-W bilayer thin films evolve in a different manner. On the one hand, W is found to *modify the wettability* of the Au top layer: The as-deposited state is characterized by a mesh-like arrangement of pre-existing critical Au film voids (and no longer isolated film islands). At 550 °C, these voids are able to grow/coalesce very easily, forming complex, particle-like structures while W acts as the substrate. On the other hand, for a reversed bilayer arrangement, W is found to suppress the dewetting of the underlying Au film because its

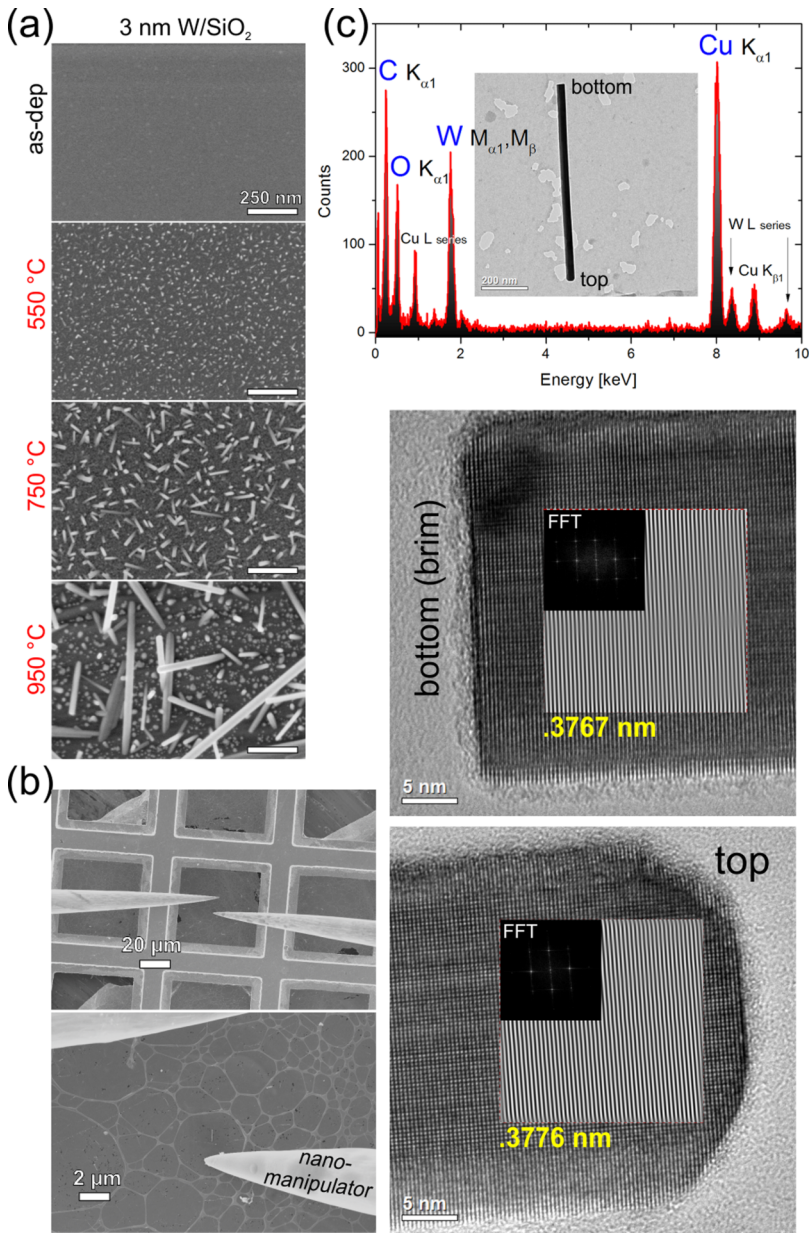

FIG. 3. Morphology evolution of ultrathin W thin films. (a) NRs are formed upon isochronal (1 min) annealing at elevated temperatures. Scale bar is valid down the column. (b) FIB nanomanipulation is used to transfer a single NR from the sample annealed at 950 °C onto a TEM grid. In the present case, the aspect ratio of the needle-like nanocrystal is approx. 22 (length ~860 nm, width ~40 nm). (c) STEM-EDS analysis shows that there is a considerably high amount of oxygen present at the region of interest (see inset). Highresolution micrographs of the bottom (brim) and the top reveal that the NR is surrounded by a thin amorphous layer covering the faceted surface. Growth direction of the single crystalline NR is highlighted by Fourier filtering and corresponds to a lattice spacing of about .377 nm. This value agrees well with the $(0\ 2\ 0)_m$ spacing of *tungsten (VI) oxide* (WO_3).

morphology is still in the initial state at 550 °C. From XRD, it is obvious that the dewetting is pending due to the passivation effect of the ultrathin W top layer. Peak evolution does not occur. As Au and W are immiscible in solid state, *phase formation* will not affect the evolution of (111) Au reflections (and the dewetting). It is rather expected that oxidation plays a major role in the dewetting. In particular, dewetting morphologies of Au on W are notably similar to that observed for other non-wetting ceramic substrates such as TiO_2.[12]

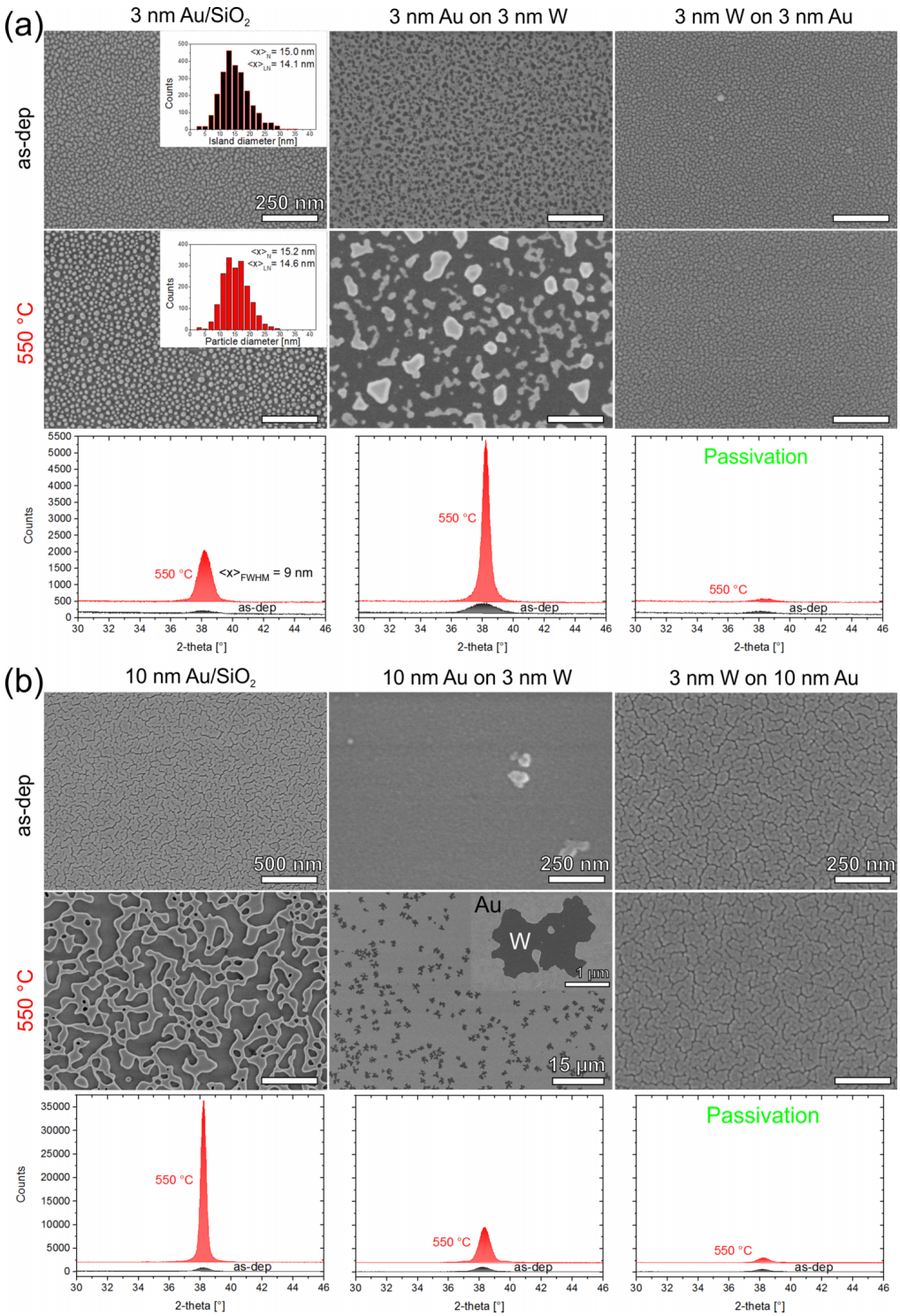

FIG. 4. Morphology evolution of Au-W bilayer thin films annealed at low temperature for 1 min. (a) Equal individual layer thickness as a function of stacking sequence. Scale bar is valid for all images. (b) Different individual layer thickness as a function of stacking sequence. Scale bars are valid down the column. Both cases show that W either acts as a substrate changing the wettability of Au or as a passivation layer suppressing the dewetting of Au thin films. The inset in (b) shows a branched Au film void exposing the underlying W film which acts as a non-wetting substrate. XRD peak intensity of Au (111) Bragg reflection can be used as a measure of the degree of coverage (due to constant Au film thickness in (a) and (b), respectively): The higher the intensity, the more substrate area has been exposed. Intensities (counts) are valid serially.

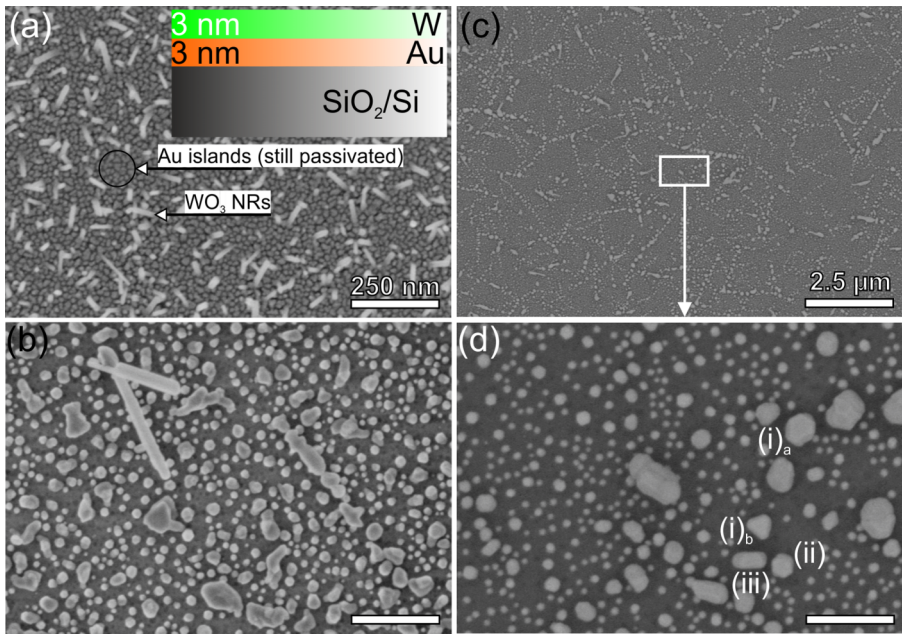

FIG. 5. Regular pattern formation of Au-WO3 NPs. (a) A 3 nm W/3 nm Au bilayer represents the starting point as illustrated. At 750 °C, oxide nanocrystal growth is initiated. (b) Upon annealing at 950 °C for 1 min, the bilayer transforms into nanoparticles (NPs) and nanorods (NRs), which are found to disintegrate. (c) Accumulated annealing at 950 °C for another 5 min then results in the formation of regular arrays of NPs. (d) Magnified view. Different kinds of particle shapes are observed alongside an individual row: (i)a,b truncated triangular profiles showing even symmetric arrangements of Au and WO3 phases, (ii) faceted, and (iii) elongated. (a) and (b) are recorded using SE contrast only; (c) and (d) use mixed signals SE/BSE in order to reduce topographical image content. Scale bar in (a) is also valid for (b) and (d).

Similar behavior is found for a different individual layer thickness. The dewetting of a 10 nm Au thin film deposited on SiO_2 is determined by the groove pattern being present in the as-deposited state. At 550 °C, pre-existing grooves seem to widen, turning the thin film into a labyrinth of exposed substrate regions. However, some critical voids may also form in the film itself. Using W/SiO_2 as the substrate makes a different situation: A grainy surface structure is seen instead of grooves or any disclosed area. Upon annealing, branched void growth is found to occur due to increased activation energies for void initiation and growth (as is usually the case for *continuous*, polycrystalline Au thin films). W being the top layer again suppresses the dewetting of Au due to the effect of passivation. A thin native oxide layer that again passivates the pure W surface will also enhance overall thin film stability. To sum up, SSD of Au thin films at low temperatures can be critically modified by changing individual layer thickness and stacking sequence of Au-W bilayer thin films (without exploiting effects due to alloying).

2. *High temperature annealing – regular pattern formation*

From all the bilayer configurations considered in this work, the most interesting one is presented in Figure 5. As shown in the previous chapters, NP formation via dewetting depends on Au film thickness: The thinner the film, the smaller the particles. Upon annealing, this process will be delayed if W is deposited onto Au/SiO_2 since it is acting as a passivation layer at low temperatures. Due to the immiscibility of Au and W even at high temperatures, effects of alloying can be neglected (which is contrary to studies such as on Au-Co bilayer films).[25] Therefore, both W and Au layers will evolve independently. The following describes how regular pattern formation of Au-WO_3 NPs is realized through self-assembly of a W/Au bilayer thin film.

Based on the findings of the present work, the following phenomenological model describes how morphology of a 3 nm W/3 nm Au/SiO_2 bilayer thin film evolves upon annealing at elevated temperatures.

(i) At medium temperature (750 °C), oxide nanocrystal growth out of the W thin film is initiated prior to the agglomeration of Au islands which are still passivated (Figure 5(a)).

(ii) Upon annealing at 950 °C, agglomeration of Au islands occurs and the growth of the WO_3 NRs is more obvious (the aspect-ratio of oxide nanocrystals is increased), as seen in the mixed morphology comprising nanoparticles (NPs) and nanorods (NRs). Moreover, some former WO_3 NRs (that undergo Rayleigh-like instabilities) are about to decompose into rows of NPs while Au islands transform into densely populated NPs (Figure 5(b)). It can be seen that the majority of the particles consists of two or more parts (*Janus-type* particles).

(iii) Upon further annealing at 950 °C, WO_3 NRs are decomposed into rows of NPs in large scale, and regular arrays of Janus-type Au-WO_3 NPs are formed (Figure 5(c)). Compositional contrast indicates that particles consist of Au and WO_3 phases which arrange in different particle shapes (Figure 5(d)). A *two-level* morphology (regular arrays of bigger particles together with smaller particles in between) is formed via self-assembly of a W/Au bilayer thin film without any chemical agents.

IV. CONCLUSIONS

This work highlights the self-assembly of Au, W, as well as Au-W thin films. The dewetting of Au films on SiO_2 emphasizes the role of film thickness with respect to the formation of NPs and their plasmonic nature. W ultrathin films are found to evolve into needle-like WO_3 NRs due to an anisotropic 1D oxide crystal growth which is not a dewetting mode in its usual manner. Adsorption of oxygen on the pure W surface is seen to play a major role for the self-assembly of W films. The aspect-ratio of oxide NRs can be easily tuned by the annealing temperature. For bilayer thin films, both W and Au are revealed to evolve independently. It is pointed out that, at low temperature, an additional thin W layer changes the dewetting nature of Au/SiO_2: W being the ground layer delays the dewetting of Au, acting as a non-wetting substrate. Oxidation of the pure W surface may also influence the dewetting nature of Au. W being the top layer even passivates the Au film and no dewetting occurs. The influence of stacking sequence was found to be substantial while individual Au layer thickness affects the degree of coverage in the as-deposited state. However, combination of Au thin film dewetting and oxide NR formation eventually results in the self-assembly of ordered arrays of Au-WO_3 NPs, potentially being used as a simple and cost-effective way to fabricate tailored Au-WO_3 nanostructures for photocatalytic applications.

ACKNOWLEDGMENTS

This work was funded by the Deutsche Forschungsgemeinschaft (DFG, Grants No. SCHA 632/20-1, and SCHA 632/24-1) and by the state of Thuringia (TMWAT, BioMacroNano2020, 2010-2012; Grant No. B715-10009). The authors thank Ms. D. Rossberg from TU Ilmenau for her help in FIB processing and Mr. M. Friák from the Institute of Physics of Materials at the Academy of Sciences of the Czech Republic. His commitment to discussing the formation of tungsten oxide nanorods is highly appreciated. The authors are also grateful to J. Uziel, G. Harnisch, B. Hartmann, I. Marquardt, and J. Döll from TU Ilmenau for their help in sample preparation. We acknowledge support for the Article Processing Charge by the German Research Foundation and the Open Access Publication Fund of the Technische Universität Ilmenau.

[1] D. Amram and E. Rabkin, ACS Nano **8**, 10687 (2014).
[2] D. Wang and P. Schaaf, Journal of Materials Chemistry **22**, 5344 (2012).
[3] N. T. Nguyen, M. Altomare, J. Yoo, and P. Schmuki, Advanced Materials **27**, 3208 (2015).
[4] A. Herz, M. Friák, D. Rossberg, M. Hentschel, F. Theska, D. Wang, D. Holec, M. Šob, O. Schneeweiss, and P. Schaaf, Applied Physics Letters **107**, 073109 (2015).
[5] C. Vidal, D. Wang, P. Schaaf, C. Hrelescu, and T. A. Klar, ACS Photonics (2015).
[6] E. Shaffir, I. Riess, and W. D. Kaplan, Acta Materialia **57**, 248 (2009).
[7] C. M. Muller and R. Spolenak, Journal of Applied Physics **113**, 094301 (2013).
[8] S.-H. Lee, E.-H. Kwak, and G.-H. Jeong, Applied Physics A **118**, 389 (2015).
[9] M.-Y. Li, Q. Zhang, P. Pandey, M. Sui, E.-S. Kim, and J. Lee, Scientific Reports **5**, 13954 (2015).
[10] A. Kosinova, O. Kovalenko, L. Klinger, and E. Rabkin, Acta Materialia **83**, 91 (2015).

[11] C. M. Müller and R. Spolenak, Acta Materialia **58**, 6035 (2010).
[12] P. D. Nsimama, A. Herz, D. Wang, and P. Schaaf, Applied Surface Science.
[13] D. Wang, R. Ji, and P. Schaaf, Beilstein Journal of Nanotechnology **2**, 318 (2011).
[14] Z. Liu, C. Lee, V. Narayanan, G. Pei, and E. C. Kan, IEEE Transactions on Electron Devices **49**, 1606 (2002).
[15] D. Amram, L. Klinger, and E. Rabkin, Acta Materialia **60**, 3047 (2012).
[16] A. Herz, D. Wang, T. Kups, and P. Schaaf, Journal of Applied Physics **116**, 044307 (2014).
[17] P. Farzinpour, A. Sundar, K. D. Gilroy, Z. E. Eskin, R. A. Hughes, and S. Neretina, Nanotechnology **23**, 495604 (2012).
[18] R. Esterina, X. M. Liu, A. O. Adeyeye, C. A. Ross, and W. K. Choi, Journal of Applied Physics **118**, 144902 (2015).
[19] W. S. Rasband, *ImageJ* (U. S. National Institutes of Health, Bethesda, Maryland, USA, 2015), at http://imagej.nih.gov/ij/.
[20] O. Kovalenko, J. R. Greer, and E. Rabkin, Acta Materialia **61**, 3148 (2013).
[21] O. Malyi, L. Klinger, D. J. Srolovitz, and E. Rabkin, Acta Materialia **59**, 2872 (2011).
[22] H. Sun, M. Yu, G. Wang, X. Sun, and J. Lian, The Journal of Physical Chemistry C **116**, 9000 (2012).
[23] S. Pokhrel, J. Birkenstock, A. Dianat, J. Zimmermann, M. Schowalter, A. Rosenauer, L. C. Ciacchi, and L. Madler, CrystEngComm **17**, 6985 (2015).
[24] H. Jehn and H. Katscher, in *Gmelin Handbook of Inorganic and Organometallic Chemistry*, 8th ed., edited by W Wolfram (Springer, Berlin Heidelberg, 1978), pp. 89–172.
[25] J. Li, D. Yin, Q. Li, C. Chen, S. Huang, and Z. Wang, Nanoscale (2015).